

Effect of nonmagnetic impurities on the Raman spectra of the superconductor niobium diselenide

R. Sooryakumar* and M. V. Klein

Materials Research Laboratory and Department of Physics, University of Illinois at Urbana-Champaign, Urbana, Illinois 61801

R. F. Frindt

Department of Physics, Simon Fraser University, Burnaby V5A 1S6, British Columbia, Canada

(Received 20 October 1980)

We recently published the results of observation of the superconducting energy gap in $2H\text{-NbSe}_2$ by Raman scattering. The gap is observed by the appearance of two new Raman-active modes of different symmetries A (18 cm^{-1}) and E (15 cm^{-1}) when the sample is immersed in superfluid helium. Theoretical calculations by Balseiro and Falicov show that these gap excitations gain their Raman activity by coupling to low-lying phonons. Crystal growth techniques, which produce nonmagnetic impurities, are known to have a small effect on superconductivity while tending to inhibit the formation of charge-density waves (CDW) in $2H\text{-NbSe}_2$. By studying such diverse samples, we present data to show the necessity of the CDW state to observe the superconducting gap excitation. The role of impurities in suppressing CDW formation is also revealed from the data.

I. INTRODUCTION

Neutron diffraction studies¹ show that $2H\text{-NbSe}_2$ undergoes a transition for a normal lattice to one with a three-wave vector incommensurate charge-density wave (CDW) at the onset temperature T_d of 33 K. The CDW is only a few percent out of commensurability and remains so to at least 1.3 K.² Below 7.2 K, $2H\text{-NbSe}_2$ is a highly anisotropic type-II superconductor.³ We recently reported the observation of the superconducting energy gap in $2H\text{-NbSe}_2$ using Raman scattering.⁴ Two new Raman-active modes of different symmetries (A and E) were seen at 2 K close in energy to the gap 2Δ . The coupling of the light to the superconducting electrons is believed to be indirect, via the Raman-active CDW phonons.⁵ This coupling was clearly evident by the behavior in a magnetic field.

A theoretical model of the new modes was given by Balseiro and Falicov.⁵ They calculated the self-energy $\pi(q, \omega)$ of a phonon of frequency $\omega_0 \approx 4\Delta$ interacting with a BCS superconductor at $T=0$. In the $q \approx 0$ limit they found an inverse square-root singularity as ω approached 2Δ from below, leading to a rather strong pole in the phonon's Greens function slightly below 2Δ .

In this paper we present experimental details and further data that support the model by proving that a CDW state is needed to make the gap excitations observable by Raman scattering. The model says the CDW is needed because of its Raman active phonon that couples to the superconducting electrons and

lends them its Raman activity. The experimental facts are brought out by a comparison of Raman scattering from diverse samples, including some with enough nonmagnetic impurities to suppress the CDW. In a separate paper,⁶ we will present further results in a magnetic field and explain them qualitatively with a simple theoretical model.

Section II will be devoted to an experimental description; the results will be presented and discussed in Sec. III.

II. EXPERIMENTAL PROCEDURE

The Raman cross section in metals is limited by the small scattering volume. Due to the metallic nature of the sample the incident light penetrates only to within the skin depth, which is estimated to be about 300 \AA in $2H\text{-NbSe}_2$.⁷ In order to couple the most amount of light to the sample, the laser beam was incident at the pseudo Brewster angle, which is about 75° . The scattered light was collected along the c axis, perpendicular to the layers. Due to the van der Waals gap separating the layers the thermal conductivity along the c axis is small, $2.5 \times 10^{-2}\text{ W/cm}^\circ\text{C}$.⁸ Laser heating in such samples has been estimated to be as much as 30–50 K for 100 mW incident power.⁸ In an effort to cut down such laser heating, the beam was spread into a line 1–3 mm long and about $30\text{ }\mu\text{m}$ wide. In runs where the sample had to be in the superconducting phase below $T_c \approx 7\text{ K}$, cooling the sample by flowing cold helium

gas was insufficient. Even with only 30 mW power, the local heating was enough to make the sample normal. To ensure that the sample was superconducting, we immersed it in superfluid helium. This in turn forced the use of low incident powers (20–30 mW) to avoid bubbling the superfluid helium.

A large part of the experiments involved working within 20 cm^{-1} of the laser frequency at 2 K. This required the use of extremely flat surfaces, to ensure very little "Rayleigh" scattering. The layered compounds are ideally suited for such work. Due to the easy cleavage of the layers by simply using plastic tape, extremely good, mirrorlike, surfaces were obtained. The availability of good surfaces avoided having to use a third monochromator or an iodine cell for stray light rejection.

By using a polaroid rotator (similar to that discussed in Ref. 8) and a quarter wave plate we could separate the Raman spectrum into its various symmetries. The spectra were recorded using a Spex model 1401 double monochromator. The signal was detected by an ITT FW130 photomultiplier tube, cooled by liquid nitrogen, which had a typical dark count of about 2–3 counts/sec. The incident laser polarization was in the plane of incidence. The light was collected in the (*XX*) and (*XY*) geometries. Typical dwell times were 30–60 sec, and the monochromator slits were set at $300 \mu\text{m}$, giving a resolution of 3 cm^{-1} at 5145 \AA . Silver epoxy was used to mount the sample on a $5 \times 5 \times 1 \text{ mm}^3$ copper plate. This in turn was attached to the end of a sample insert by G. E. 1701 varnish for better thermal contact. The thermocouple and or germanium resistor were fastened on the insert close to the sample. The sam-

ple was cooled in a Janis Varitemp cryostat. It was possible to control the temperature to within 1 K by using a heater and adjusting the needle value which allows liquid helium into the sample chamber. Between runs the sample chamber was evacuated by a liquid-nitrogen-trapped, two-stage, mechanical pump. When the chamber was filled with static helium gas while the sample was cold, the sample surface was observed to "deteriorate," in the sense that elastic light scattering increased. Apparently dust or small aggregates of frozen gas were condensing on the surface. This effect irreversibly spoiled the surface for close-in Raman scattering.

III. SAMPLE CHARACTERIZATION

The Raman scattering results that will be presented in this section have been carried out on a large number of samples of $2H\text{-NbSe}_2$ provided from various different sources. Their properties are tabulated in Table I. Different growth procedures and impurity contents affect the CDW formation.^{9–11} The effect on the superconducting transition temperature, however, is small.^{12,13}

A. Raman scattering results: Samples M and B

The room-temperature Raman spectrum on sample M was obtained by Holy¹⁴ and is reproduced in Fig. 1. Our own measurements at room temperature on this sample were not possible since M was "used up"

TABLE I. Samples of $2H\text{-NbSe}_2$.

Sample	Source	r^a	T_c (K)	Properties of CDW phonon
M	S. F. Meyer (Univ. of Illinois)		~7	Strong well-defined <i>A</i> and <i>E</i> phonons. <i>A</i> is centered at 40 cm^{-1} and <i>E</i> at 45 cm^{-1} .
B	F. J. DiSalvo (Bell Labs)	0.02	~7	Strong <i>A</i> phonon at 36 cm^{-1} . <i>E</i> is weak and broad with maximum around 43 cm^{-1} .
D	R. F. Frindt (Simon Fraser Univ.)	0.17	~7	No CDW
E	R. F. Frindt	0.105	~7	No CDW
E'	R. F. Frindt	0.105	~7	Very weak <i>A</i> mode centered at 32 cm^{-1} . <i>E</i> mode not clearly seen.

^a Residual resistance ratio $R(8 \text{ K})/[R(300 \text{ K}) - R(8 \text{ K})]$, along the layers, measured on samples from the same growth batch.

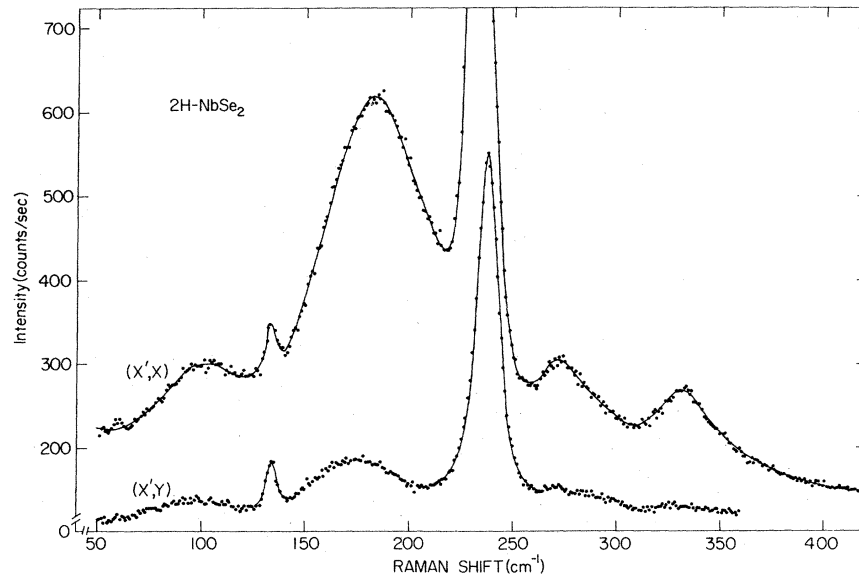


FIG. 1. (Reproduced from Ref. 14). Polarized spectra of $2H\text{-NbSe}_2$ (sample M) at room temperature. Laser power = 300 mW, resolution = 4 cm^{-1} , dwell time = 20 sec. The A_{1g} mode at 230 cm^{-1} and E_{2g} mode at 237 cm^{-1} are off scale in the $(X'X)$ scan.

by repeated cleavings which were essential for the low-temperature runs. The first-order Raman modes are at 230 cm^{-1} (A_{1g}) and 237 cm^{-1} (E_{2g}). A two-acoustic-phonon peak is seen at 180 cm^{-1} [FWHM (full width at half maximum) = 50 cm^{-1}] in the (XX) spectrum and at about 175 cm^{-1} in (XY) . Optical two-phonon peaks are seen at 272 and 330 cm^{-1} in the A symmetry. The 133 cm^{-1} peak results from leakage of the E_{1g} mode, and the broad feature around 100 cm^{-1} is due to impurities in the sample. The two-phonon peak has previously been noted and discussed by Maldague and Tsang.¹⁵ Similar Raman spectra were obtained by us for all the other NbSe_2 samples at room temperature (Figs. 7–12).

The frequency of the broad, strong two-phonon peak is approximately twice that of the “anomaly” in the dispersion curve for the longitudinal acoustic (LA) phonon.¹⁶ The anomaly appears as a maximum followed by a minimum near $q = \frac{2}{3}\Gamma M$. This curve was measured on sample D, which, has no CDW.^{9,11} We interpret the two-phonon peak as a combination of 2 LA phonons of wave vector $+\bar{q}$, and $-\bar{q}$ where \bar{q} is near $\frac{2}{3}\Gamma M$. A similar strong two-phonon Raman peak is seen in $2H\text{-TaSe}_2$.^{14,15}

On cooling sample M, the first-order phonons harden and move to 234 cm^{-1} (A_{1g}) and 249 cm^{-1} (E_{2g}) at 10 K. The E_g phonon broadens. The two-phonon structure at 180 cm^{-1} softens and loses intensity. It is centered around 160 cm^{-1} at 100 K.

Just above the incommensurate phase transition at $T_d \approx 33\text{ K}$, the broad peak is no longer observable. Below T_d the CDW distortion induces A and E Ra-

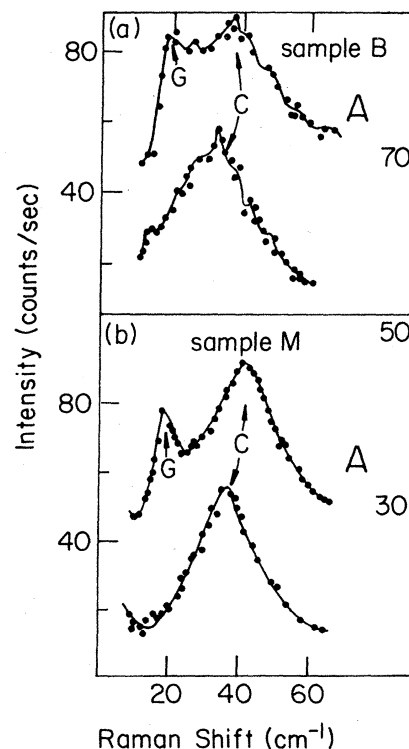


FIG. 2. Raman spectra from samples B and M [(a), (b)] at two different temperatures, 9 K (lower curve in each pair) and 2 K (upper curves) for A symmetries. C: CDW modes, G: new peak. The solid curve drawn through the data for sample M was hand drawn; that in B is the result of a five-point computer smoothing operation.

man active phonons to appear. On further cooling they harden and get stronger. These modes were first seen by Tsang *et al.*,¹⁷ though they did not separate their spectrum into A and E components. The low-temperature spectra for samples M and B are shown in Figs. 2 and 3. Figure 2 shows two pairs of Raman spectra [(a), (b)] from the samples at two different temperatures, 9 (lower curve in each pair) and 2 K (upper curves) for A symmetry. Figure 3 shows the same for E symmetry. On comparing the 9 and 2 K results, we see that two new peaks G of A and E symmetry are present when the sample is immersed in superfluid helium. This is believed to arise from the superconducting properties of the sample.^{4,5} The CDW induced amplitude modes are labeled "C," while "I" shows the interlayer mode.¹⁸ There is no change in the spectrum between 9 and 2 K for frequencies greater than 70 cm^{-1} .

The A spectrum is obtained by subtracting the $(X'Y)$ spectrum from $(X'X)$. The $(X'Y)$ spectrum gives the E symmetry directly. We note that there are two distinct CDW peaks of different symmetry. Furthermore, even in the incommensurate phase, where the unit cell is infinite, we are still able to assign specific symmetries (A and E) to the spectrum. These observed pure selection rules imply that the "local" structure in the incommensurate phase

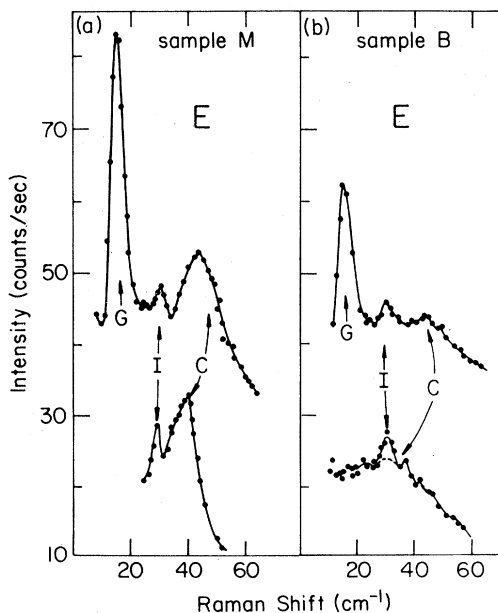


FIG. 3. Raman spectra from samples B and M at different temperatures 9 K and 2 K for E symmetries. C: CDW modes, G: new peaks, I interlayer mode. The solid curve drawn through the data for sample M was hand drawn; that in B is a result of a five-point computer smoothing operation.

has approximately three-fold or six-fold rotational symmetry. In such a case, the Raman cross section would give separate A and E amplitude modes of the three-wave vector incommensurate CDW. This follows directly from the polarizability tensors for D_{6h} and D_{3d} .

It is noted that for sample B the CDW E mode is very much weaker and broader than the corresponding E mode of M. Furthermore the position of the new peaks G is essentially sample independent, whereas the position and strength of the CDW modes (C) are sample dependent. This may be explained by the work of Huntley¹⁰ and Long *et al.*,¹³ where it was shown that crystal growth techniques, which produce nonmagnetic impurities, have a small effect on superconductivity while tending to inhibit the formation of CDW's. This is indicative that G may be due to the superconducting properties of $2H\text{-NbSe}_2$. The positions of the Raman peaks agree closely with the BCS energy gap. At 1.6 K, this gap is given by $2\Delta = 17.2 \pm 0.4 \text{ cm}^{-1}$ as determined by the position of a far infrared absorption peak.¹⁹ The weighted average of the new Raman peaks is 16 cm^{-1} and essentially agrees with the position of the infrared peak.

B. Samples D, E, and E'

The above-mentioned coupling of the CDW modes to peaks G raises the interesting question, namely, the consequences to G if this coupling is turned off. Turning off the interaction between C and G is difficult to achieve experimentally. It may be approached by gradually decreasing the CDW transformation while maintaining the superconducting properties of the sample. Pressures up to 30 kbar are known to suppress the CDW formation¹² while increasing T_c , the superconducting transition temperature by 0.8 K.

We have approached this by studying $2H\text{-NbSe}_2$ samples with nonmagnetic impurities. Such impurities are known to inhibit CDW formation. In particular, Raman measurements have been made on several samples studied by Huntley and Frindt⁹ and by Stiles *et al.*¹¹ which have no CDW's but are still superconductors below 7 K. We studied samples from batches E and D of Ref. 9. Hall coefficient⁹ measurements carried out on these samples show no reversal of sign above 5 K and hence no CDW. The NMR spectra show no CDW-produced broadening.¹¹

Figure 4 shows the A and E Raman spectrum of sample D when immersed in superfluid helium. The E spectrum has been displaced for clarity. There is no evidence of the CDW phonons C nor the gap modes G . I is the interlayer mode, while peak B is due to scattering from superfluid helium. Its position agrees with the result of Greytak and Yan.²⁰ In sample B this mode is hidden by the stronger gap mode G . More discussion on peak B is presented with the

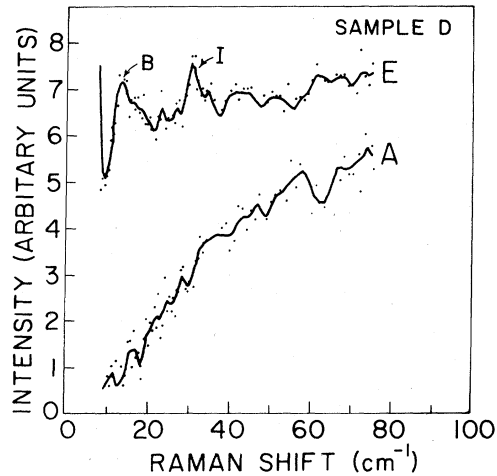


FIG. 4. *E* and *A* symmetry Raman spectra from $2H$ - $NbSe_2$ (sample D) when immersed in superfluid helium. The solid curve represents a five-point computer smoothing of the data. *B*: scattering from superfluid helium. *I*: inter-layer mode.

magnetic field results.⁶ The nearly linear rise of the scattering cross section for $\omega < 50 \text{ cm}^{-1}$ is characteristic of the electronic scattering predicted for free carriers.²¹ For low temperatures and small q one expects the free electron spectrum to be proportional to ω for $\omega < qv_f$. Owing to the complexity of the Fermi surface and the nonconservation of momentum perpendicular to the metal surface, it is difficult to estimate the Fermi velocity v_f and the appropriate value of q . There seems to be no evidence of any direct excitations across the BCS gap in sample D.

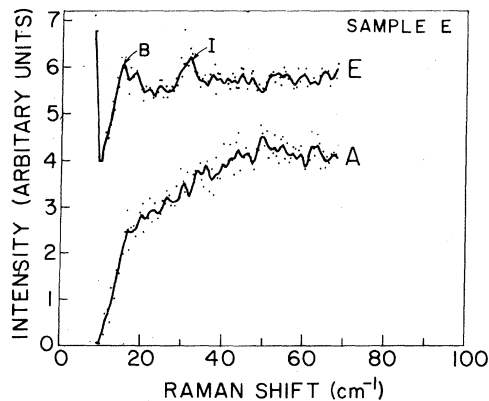


FIG. 5. *E* and *A* symmetry Raman spectra from $2H$ - $NbSe_2$ (sample E) when immersed in superfluid helium. The solid curve represents a five-point computer smoothing of the data. *B*: scattering from superfluid helium. *I*: inter-layer mode.

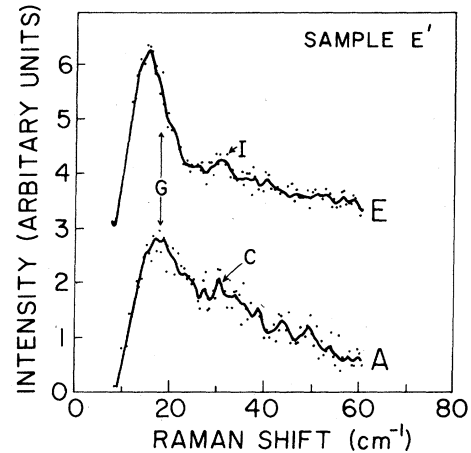


FIG. 6. *E* and *A* symmetry Raman spectra from $2H$ - $NbSe_2$ (sample E') when immersed in superfluid helium. The solid curve represents a five-point computer smoothing of the data. *G*: new mode; *C*: weak CDW mode; *I*: inter-layer mode.

Sample *E* studied by Frindt *et al.*, behaves similar to D and is shown in Fig. 5. The *E* spectrum again shows only modes *I* and *B*. The *A* spectrum however seems to have a steep rise below 16.5 cm^{-1} and then a slower linear rise. The change in slopes could be due to superconductivity and might represent the predicted intrinsic scattering from a superconductor.²²⁻²⁷

One of the samples we studied from batch E (called E') however did show the new peaks *G*. The spectrum is shown in Fig. 6. We believe this is due to the presence of a smeared out CDW phonon, and this weak *A*-symmetry phonon is indicated by *C*. There is less evidence for the corresponding *E*-symmetry CDW mode. The superfluid helium peak *B* is hidden by the stronger gap mode *G*.

C. Comparison between B, D, and E'

The complete *E* and *A* spectra for samples D, E', and B for various temperatures from room temperature to 2 K are shown in Figs. 7-12. In each figure the solid curve superimposed on the 10 K run corresponds to the spectrum when the sample is immersed in superfluid helium. This superposition of the spectra was made in order to observe the change in intensity more clearly when the temperature changes from 10 to 2 K. All temperatures shown are as indicated by the thermocouple. No correction has been made for laser heating which, for the 10, 100, and 300 K curves could be between 5-10 K for the powers used. All counting rates were normalized to

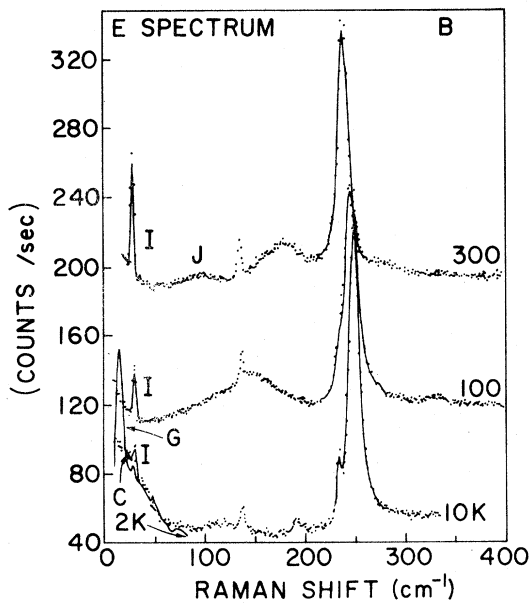


FIG. 7. *E*-symmetry Raman spectra from sample B. The temperatures are as indicated by the thermocouple. No correction for laser heating has been made. Power = 30 mW, resolution = 3 cm^{-1} at 5145 Å. The curves at 100 and 300 K have been displaced by 80 and 160 cts/sec, respectively. *G*: new mode; *C*: CDW mode; *I*: interlayer mode; *J*: impurity- or defect-induced modes.

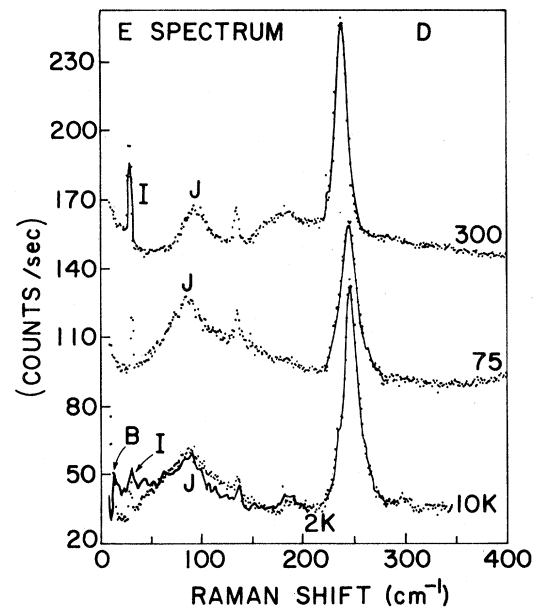


FIG. 9. *E*-symmetry Raman spectra from sample D. The temperatures are as indicated by the thermocouple. No correction for laser heating has been made. Power = 30 mW, resolution = 3 cm^{-1} at 5145 Å. The curves at 75 and 300 K have been displaced by 60 and 120 cts/sec, respectively. *B*: scattering from superfluid helium; *I*: interlayer mode; *J*: impurity- or defect-induced modes.

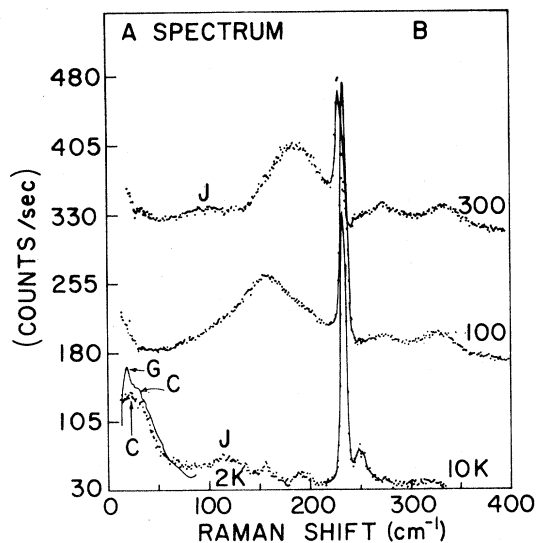


FIG. 8. *A*-symmetry Raman spectra from sample B. The temperatures are as indicated by the thermocouple. No correction for laser heating has been made. Power = 30 mW, resolution = 3 cm^{-1} at 5145 Å. The curves at 100 and 300 K have been displaced by 150 and 300 cts/sec, respectively. *G*: new mode; *C*: CDW modes; *J*: impurity- or defect-induced modes.

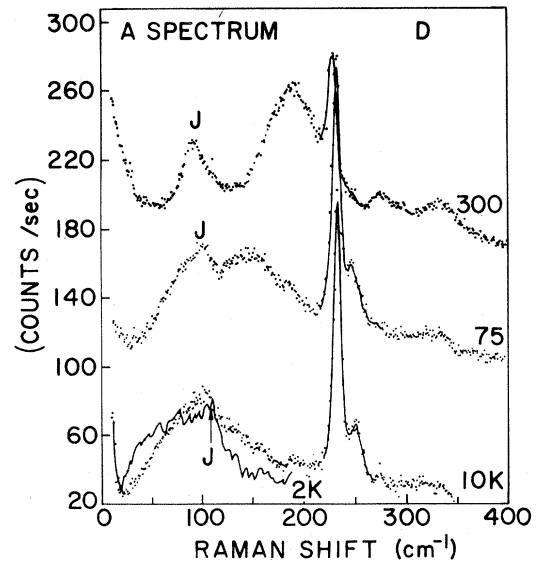


FIG. 10. *A*-symmetry Raman spectra from sample D. The temperatures are as indicated by the thermocouple. No correction for laser heating has been made. Power = 30 mW, resolution = 3 cm^{-1} at 5145 Å. The curves at 75 and 300 K have been displaced by 80 and 160 cts/sec, respectively. *J*: impurity- or defect-induced modes.

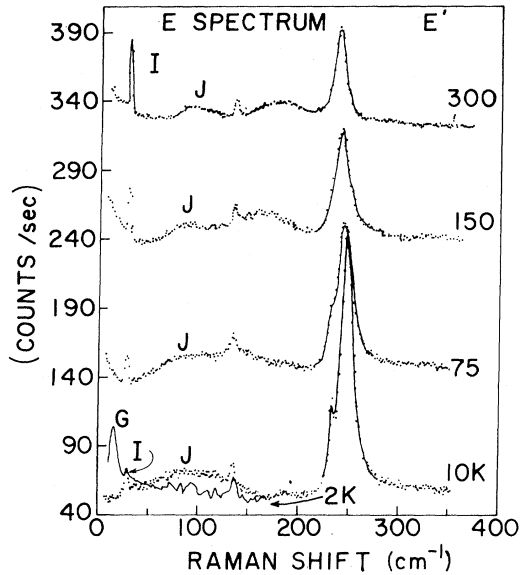


FIG. 11. *E*-symmetry Raman spectra from sample *E'*. The temperatures are as indicated by the thermocouple. No correction for laser heating has been made. Power = 30 mW, resolution = 3 cm^{-1} at 5145 \AA . The curves at 75, 150, and 300 K have been displaced by 100, 200, and 300 cts/sec, respectively. *G*: new mode; *I*: interlayer mode; *J*: impurity- or defect-induced modes.

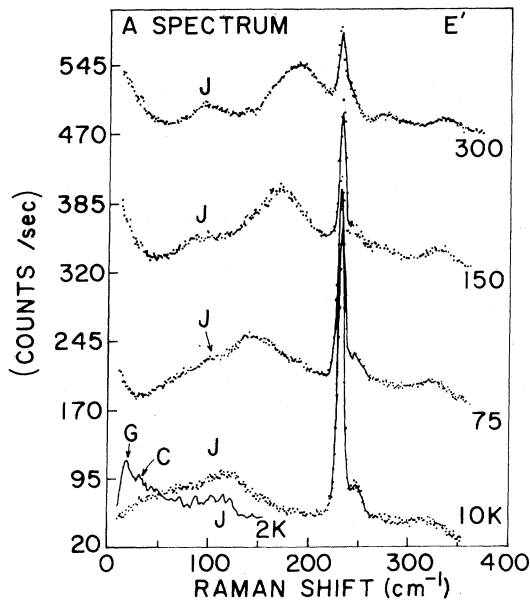


FIG. 12. *A*-symmetry Raman spectra from sample *E'*. The temperatures are as indicated by the thermocouple. No correction for laser heating has been made. Power = 30 mW, resolution = 3 cm^{-1} at 5145 \AA . The curves at 75, 150, and 300 K have been displaced by 150, 300, and 450 cts/sec, respectively. *G*: new mode; *C*: CDW mode; *J*: impurity- or defect-induced modes.

an incident laser power of 30 mW. There may be slight variations from run to run in the absolute scale of the intensity value due to unavoidable differences in beam focusing, changes in sample surface quality and consequent changes in the amount of incident energy absorbed.

Sample B used for runs in Figs. 7 and 8 was from the same batch as that used in the magnetic field studies.^{4,6} In B, which is considered a "good" sample, we observe the expected softening of the 170–180 cm^{-1} two-phonon *A* and *E* peaks from 300 K. These peaks are not seen at 10 K. They soften, and at 33 K the lattice distorts in the CDW state. The weak broad structure *J* around 100 cm^{-1} at room temperature is seen to harden somewhat and is at about 115 cm^{-1} at 10 K. We attribute this mode to impurity scattering. The formation of CDW modes *C* is seen at 10 K. At 2 K modes *G* appear.

In sample D, the impurity modes *J* are much stronger and narrower than in B. In fact for the *E* symmetry—Fig. 9—mode *J* is stronger than the two-phonon mode. On cooling, the two-phonon modes in the *A* and *E* spectrum do soften and lose intensity. However, the softening is not complete, and at 10 K the two-phonon peak is hidden under *J*. Cooling to 2 K softens the two-phonon modes further and there is evidence in the *A* spectrum (Fig. 10) that it is now centered around 75 cm^{-1} . The *E* spectrum shows a shoulder on the low-energy side of *J*, suggesting further softening of the two phonon mode.

The softening of the acoustic phonons is seen indirectly through the two phonon peak. Neutron diffraction data on $2H\text{-TaSe}_2$ (Ref. 16) show a similar effect. The fact that these modes do not soften completely in D implies there is no distortion to the CDW phase. This supports other measurements made on D.^{9,11} At 2 K, scattering from superfluid helium is observed in sample D. This is not clearly observed in the other samples due to overlap with the gap modes *G*.

The acoustical two-phonon softening and decrease in intensity in sample *E'*—Figs. 11 and 12—is similar to that in D. However, these modes, which still seem to be present at 10 K, soften further and have disappeared at 2 K. The lattice presumably distorts to the CDW state at a lower temperature than in B. The gap modes *G* are weaker in intensity than in Fig. 7, though occurring at the same frequency. Impurity modes *J* in *E'*, although stronger than B, are less pronounced when compared to D. At low temperatures, *J* is centered around 110 cm^{-1} .

The role of impurities in the formation of the CDW state is seen clearly from these results. At some critical concentration and type of impurity (close to that in *E'*)¹¹ the scattering of electrons from defects is strong enough to overcome the static electron-phonon coupling necessary for the formation of CDW's. The impurity effects in these particular

samples are thought to be due to⁹ iodine and structural defects, which depend on growth procedures and conditions. These results are not inconsistent with previous results of neutron¹⁶ and Raman¹⁷ scattering from CDW phonons where nearly complete softening of the acoustic phonons marks the onset of CDW's.

In conclusion we see that to observe the new modes G , the presence of a CDW is necessary, presumably because of its low-lying Raman active mode C . As pointed out by Balseiro and Falicov,⁵ the modes should be observable in non-CDW superconductors if there is a Raman active mode close enough to couple strongly to the electrons. This, however, should satisfy the further condition

$$q \ll 2\Delta/(\hbar v_f), = 2\pi/\xi_0, \quad (1)$$

where v_f is the Fermi velocity, ξ_0 is the BCS coher-

ence length, and q the wave vector of the phonon which is determined by the light-scattering kinematics.^{28,29} The interlayer mode I seen in $2H-NbSe_2$ does not seem to be affected by the electrons and hence probably does not satisfy the strong-coupling condition.

ACKNOWLEDGMENTS

We thank S. F. Meyer, F. J. DiSalvo, and R. V. Coleman for providing crystals. Thanks go to W. L. McMillan and John Bardeen for theoretical discussions and to L. M. Falicov for many conversations and for his patient explanation of the theory of Ref. 5. This work was supported by the National Science Foundation under the MRL Grant No. DMR-77-23999 and the National Science and Engineering Research Council of Canada.

*Present address: Max-Planck-Institut für Festkörperforschung, Heisenbergstrasse 1, 7000 Stuttgart 80, West Germany.

¹D. E. Moncton, J. D. Axe, and F. J. DiSalvo, Phys. Rev. B **16**, 801 (1977).

²M. Barmatz, L. R. Testardi, and F. J. DiSalvo, Phys. Rev. B **12**, 4367 (1975).

³P. de Trey, Suso Gygax, and J. P. Jan, J. Low Temp. Phys. **11**, 421 (1973).

⁴R. Sooryakumar and M. V. Klein, Phys. Rev. Lett. **45**, 660 (1980).

⁵C. A. Balseiro and L. M. Falicov, Phys. Rev. Lett. **45**, 662 (1980).

⁶R. Sooryakumar and M. V. Klein, Phys. Rev. B **23**, 3213 (1981) (preceding paper).

⁷R. T. Harley and P. A. Fleury, J. Phys. **12**, L863 (1979).

⁸D. G. Bruns, Ph.D. dissertation (University of Illinois, Urbana, 1979) (unpublished).

⁹D. J. Huntley and R. F. Frindt, Can. J. Phys. **52**, 861 (1974).

¹⁰D. J. Huntley, Phys. Rev. Lett. **36**, 490 (1976).

¹¹J. A. R. Stiles, D. L. Williams, and M. J. Zuckermann, J. Phys. C **9**, L489 (1976).

¹²C. Berthier, P. Molinie, and D. Jerome, Solid State Commun. **18**, 1393 (1976).

¹³J. R. Long, S. P. Bowen, and H. E. Lewis, Solid State Commun. **22**, 363 (1977).

¹⁴J. A. Holy, Ph.D. dissertation (University of Illinois, Urbana, 1977) (unpublished).

¹⁵P. F. Maldague and J. S. Tsang, in *Proceedings of the International Conference in Lattice Dynamics*, edited by M. Balkanski (Flammarion, Paris, 1978), p. 607.

¹⁶D. E. Moncton, J. D. Axe, and F. J. DiSalvo, Phys. Rev. Lett. **34**, 734 (1975).

¹⁷J. C. Tsang, J. E. Smith, Jr., and M. W. Shafer, Phys. Rev. Lett. **37**, 1407 (1976).

¹⁸C. S. Wang and J. M. Chen, Solid State Commun. **14**, 1145 (1974).

¹⁹B. P. Clayman and R. F. Frindt, Solid State Commun. **9**, 1881 (1971).

²⁰T. J. Greytak and J. Yan, Phys. Rev. Lett. **22**, 987 (1967).

²¹M. V. Klein, in *Light Scattering in Solids*, edited by M. Cardona (Springer-Verlag, New York, 1975).

²²A. A. Abrikosov and L. A. Falkovskii, Sov. Phys. JETP **13**, 179 (1961).

²³A. A. Abrikosov and V. M. Genkin, Sov. Phys. JETP **38**, 417 (1974).

²⁴S. Y. Tong and A. A. Maradudin, Mater. Res. Bull. **4**, 563 (1969).

²⁵D. R. Tilley, Z. Phys. **254**, 71 (1972); J. Phys. F **3**, 1417 (1973).

²⁶C. B. Cuden, Phys. Rev. B **13**, 1993 (1976).

²⁷C. B. Cuden, Phys. Rev. B **18**, 3156 (1978).

²⁸A calculation of the phonon spectral function of an acoustic phonon has been made by Schuster [Solid State Commun. **13**, 1559 (1973)] in the large q limit where $v_f q \gg 2\Delta/\hbar$. In this large q -limit and with a simple Fermi surface the inverse square root singularity of the real part of the phonon self-energy found by Balseiro and Falicov (Ref. 5) for $\omega = 2\Delta/\hbar$ becomes a logarithmic singularity. As with their results for the spectral function, Schuster's calculation gives structure around 2Δ . However, strong modifications of the spectra appear only when 2Δ is extremely close to $\hbar\omega_q$. For $2\Delta \sim \hbar\omega_q/2$ (as in our experimental results) the effects are essentially negligible. It thus appears that the experiments require the small q limit if the indirect phonon-coupling model is to work.

²⁹Coherence lengths for $2H-NbSe_2$ have been calculated from critical-field data by P. de Trey, Suso Gygax, and J. P. Jan, J. Low Temp. Phys. **11**, 421 (1973). They find $\xi_{\parallel} = 77 \text{ \AA}$ parallel to the layers and $\xi_{\perp} = 23 \text{ \AA}$ perpendicular to the layers. We estimate from our light-scattering geometry that $q_{\parallel} = 1.2 \times 10^5 \text{ cm}^{-1}$ and use a $q_{\perp} \sim \delta^{-1} = 5 \times 10^5 \text{ cm}^{-1}$, where δ , the optical skin depth, has been measured by R. T. Harley and P. A. Fleury, J. Phys. C **12**, L863 (1979). These values satisfy the inequality (1) by more than an order of magnitude. These considerations concerning q assume the "clean limit" where ξ_0 is larger than the mean free path l , which is difficult to estimate from the resistivity in a material with a complicated Fermi surface.